2022 IEEE Nigeria 4th International Conference on Disruptive Technologies for Sustainable Development (NIGERCON) | 978-1-6654-7978-3/22/$31.00 ©2022 IEEE | DOI: 10.1109/NIGERCON54645.2022.9803182

Performance Analysis of a PMSM for Traction Applications in Electric Vehicles with Hairpin Winding Technology

Omokhafe J. Tola , James G. Ambafi
Department of Electrical and Electronic Engineering
Federal University of Technology
Minna, Nigeria
omokhafe@futminna.edu.ng,
ambafi@futminna.edu.ng

Edwin A. Umoh
Department of Electrical and Electronic Engineering Technology
Federal Polytechnic
Kaura Namoda, Nigeria
eddyumoh@gmail.com

Olusegun E. Osinowo
Department of Electrical Engineering
NTA Channel 10
Lagos, Nigeria
olusegunosinowo1@gmail.com

***Abstract*—This paper presents the performance analysis of an interior permanent magnet synchronous motor (IPMSM) for electric vehicle application based on hairpin winding technology. Firstly, the vehicle dynamic was modelled and analysed to determine an appropriately rated motor for the drive system, and a suitable IPMSM via finite element analysis (FEA) using hairpin winding in the stator. Four different layers of hairpin winding – 2-layer, 4-layer, 6-layer and 8-layer were considered. The performance analysis show that the 8-layer has the lowest mechanical losses, and thus most suitable for application in electric vehicles design.**

Keywords — IPMSM; hairpin winding technology, electric vehicle; finite element analysis

I. INTRODUCTION

Fossil fuel-based vehicles are a major source of air pollution in the environment. Furthermore, combustion engine vehicles are not suitable for the environment. Electric vehicles (EV) have become viable alternatives in recent years. An electric motor is one of the significant design modules of the electric vehicle. However, two major challenges to EV are minimal power requirements for propulsion and energy utilization. Thus, optimum selection of electric motor with less ripple torque, lighter weight, less noise, and high efficiency can result in less periodic maintenance and increase in vehicular life span. Permanent magnet synchronous motors (PMSM) are considered owing to high efficiency; torque density and good performance in the field-weakening section[1][2]. However, the rotating portion of the PMSM which is made up of permanent magnet (PM) materials can be demagnetized suddenly due to high remnant flux density and high operating temperature during operation. This can be overcome by the application of hairpin winding with suitable conductor bars.

The demand for highly efficient electric traction motors is set to rise as the forecast reaches a 30% market share in 2030 of the increasing number of electric vehicles [3]. Recent research works have focused on electric proportion due to the need to decarbonize the society. Electric motor and its component play a vital role in this respect. The EV traction with hairpin winding technology in the stator is gaining attention among researchers due to the associated intrinsically high slot fill factor, good thermal indulgence and short end-winding length which makes the winding a good candidate for traction applications. However, the major drawback is high losses at high-frequency operation due to skin and proximity effects. The winding consists of pre-shaped copper bars that are modelled into a hairpin shape which are subsequently inserted into the stator slot.

Hairpin windings have generated tremendous interest in high torque density electric vehicle applications [4], [5]. However, compared to the conventional round conductors, dc copper loss due to the shortened end-winding and a higher fill factor leads to high current density, peak torque, and a fully automated manufacturing process that eventually reduces associated costs [6]. Studies on ripple torque reduction [7], and reduction of AC winding losses at high frequency by varying the number of conductor layers from four to six, and the effect of skin and proximity effects were decreased. [8].

This study focuses on the performance analysis of an IPMSM for vehicle traction application with hairpin winding using different conductor bar of the layer is considered. In this design approach, the performance of the IPMSM is considered by analyzing the AC losses at high frequency.

II. METHODOLOGY

A. Electric Vehicle Dynamic Analysis

The dynamic analysis of the vehicle is persistent by the consequential forces adoptive on the vehicle as given in (1). The tractive energy as of the wheel depends on the motor torque, gear ratio, and the motor's efficiency. Therefore, tractive force ought to stunned the total force applied on the vehicle when moving, which depending on the motor power together with gear ratio and the wheel radius [9]–[11].

$$M_v a_v = F - \sum F_r \tag{1}$$

Where M_v is mass of the vehicle, a_v is vehicle acceleration, F is the tractive force or the road load of the electric vehicle and F_r is the resistive force.

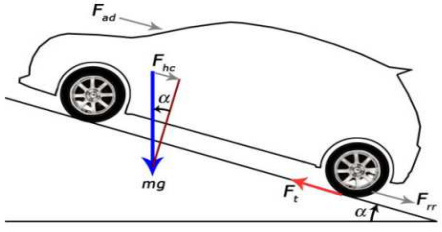

Fig. 1: Tractive forces acting on the vehicle on a slope

978-1-6654-7978-3/22/$31.00 ©2022 IEEE

The driving power is determined from the overall force applied on the vehicle when moving, as shown in Fig. 1. The total resistive forces are given as

$$F_r = F_{rr} + F_{hc} + F_{ad} \quad (2)$$

where F_{rr} is the rolling force, F_{hc}climbing resistance and F_{ad} drag force. The rolling force is a function of the pressure in the surface area between the road and the tires and is given as

$$F_{rr} = C_{roll} M_r g cos\alpha \quad (3)$$

where

$C_{roll} = \left(1 + \frac{v}{160}\right)$ and α is the slope angle of the road. The hill-climbing force is called gradient force, and be subject to the mass of the vehicle and acceleration due to gravity. The relationship between the climbing angle and the power of the vehicle is shown in Fig. 2. Once the vehicle travels on a plane road, the force is zero due to inclination angle which is zero.

$$F_{hc} = \pm M_v g sin\alpha \quad (4)$$

Where the positive sign indicates a climbing force and the negative sign indicates a downgrade force. The speed and torque of the vehicle are inversely proportional; therefore, the speed should be reduced to maintain the torque.

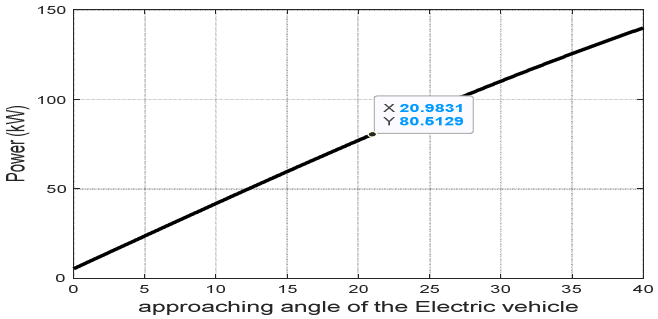

Fig. 2: Climbing angle and power relationship

Aerodynamic drag force is due to air resistance when the vehicle moves and is opposite the vehicle's direction. The force is expressed as [12], [13].

$$f_{ad} = \frac{1}{2}\rho A_f C_d v^2 \quad (5)$$

where ρ is the air density, A_f front area of the vehicle, C_d aerodynamic drag force coefficient whereas v is speed of the wind. Therefore, aerodynamic drag force is directly proportional to the vehicle's speed, as presented in Fig. 3.

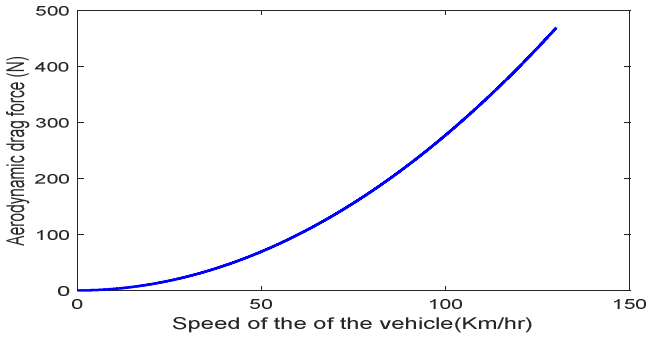

Fig. 3: Aerodynamic drag force and speed of the vehicle

The mechanical power, which includes the transmission losses, must be greater than the traction power determined. The power required to drive the EV compensates for the road load using the vehicle parameters. As the speed of the vehicle increase, the traction power increases as well, but it cannot custom the overall mechanical driving power. In this study, a 60kW IPMSM is chosen to drive the vehicle based on the association flanked by the mechanical power and the vehicle's speed, as presented in Fig. 4. As seen, that the vehicle reaches maximum speed without using the total mechanical power as the speed increase and power increases also. The motor drive characterises when used as EV proportion is presented in Fig. 5. Mechanical power should be less than the optimal power, and the speed increases up to a based speed of the chosen motor to reduce the cost, volume, and weight and maintain optimum power. The proposed parameters for EV performance are presented in Table I.

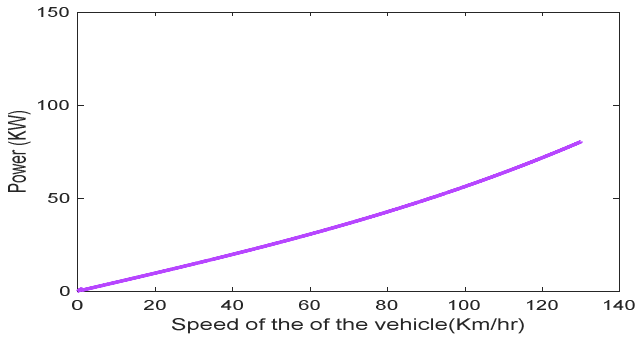

Fig. 4: Mechanical power and speed relationship

The peak power task is crucial in performance analysis from the particular of EV. Therefore, low and high speed the two operating conditions designated to examine the losses of the motor in the peak power operation, as seen in Fig. 5.

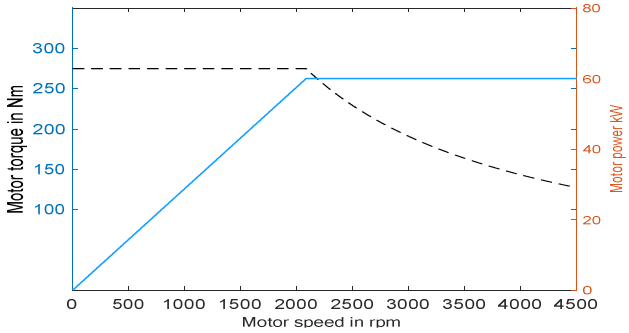

Fig. 5: Torque/Power –Speed curves

Design parameters used for the electric vehicle are tabulated in Table I.

III. PMSM MODEL

The model equations of the proposed machine in the $d-q$ reference frame are expressed as voltage, flux linkage and torque equations. It is assumed from the ideal model that: damping not be present in the rotor, eddy currents, hysteresis losses and saturation are ignored, back emf is perfectly sinusoidal, and 3-Φ windings are symmetrical, where the $d-q$ axes are constant and independent of the current but not in reality.

Table I: Electric Vehicle Data

Data	m = 1500kg, C_{roll} = 0.015, C_d = 0.3, A_f = 2 m^2, R=0.25324m
Acceleration	0 - 80 km/h in 10 sec on level ground
Speed	V_{max} =130km/h, V_{rated} =100km/h
Transmission:	η =95%
Power	P_{max} =100 kW, P_{rated} = 60 kW
Torque	T_{max} = 450Nm, T_{rated} = 275 Nm
Maximum gradient	26 degree

In the model equations, the cross-saturation between the d-q axes is obvious owing to the limitation of the symmetry design of the machine. Moreover, it is noted that the $d-q$ axes flux linkages are a function of the $d-q$ axes current [14], [15] [16].

$$\begin{cases} v_d = ri_d + \frac{d\lambda_d}{dt} - \omega_r\lambda_q \\ v_q = ri_q + \frac{d\lambda_q}{dt} - \omega_r\lambda_d \end{cases} \quad (6)$$

$$\lambda_d = L_d(i_d, i_q)i_d + \lambda_{pm} + L_{dq}i_q \quad (7)$$

$$\lambda_q = L_q(i_d, i_q)i_q + L_{qd}i_d \quad (8)$$

where i_d, i_q v_d, v_q, and λ_d λ_q are current, voltage and flux linkage in d-q axis, respectively. Furthermore ω_r is the angular speed and r being the winding resistance. L_{dq} and L_{qd} are mutual inductances of $d-q$ -axes winding with respect to $d-q$ -axes. The electromagnetic torque of the motor where cross-coupling is taken into consideration is given as [15]

$$T_e = \frac{3}{2}P\left[\lambda_d(i_d, i_q)i_q - \lambda_q(i_d, i_q)i_d\right]$$

$$= \frac{3}{2}P\left[\lambda_d(i_d = 0, i_q)i_q + \frac{\lambda_d(i_d, i_q) - \lambda_d(i_d = 0, i_q)}{i_d} i_d, i_q - \frac{\lambda_d(i_d, i_q)}{i_q} i_d, i_q\right]$$

$$= \frac{3}{2}P\left[\lambda_{pm}(i_q)i_q + L_d(i_d, i_q) - L_q(i_d, i_q)i_d i_q\right] \quad (9)$$

where

$$\lambda_{pm}(i_q) = \lambda_d(i_d = 0, i_q) \quad (10)$$

$$L_d(i_d, i_q) = \frac{\lambda_d(i_d, i_q) - \lambda_{pm}(i_q)}{i_d} \quad (11)$$

$$L_q(i_d, i_q) = \frac{\lambda_d(i_d, i_q)}{i_q} \quad (12)$$

The negative sign of the equation indicates that the d-axis current produces a counter torque to the machine [17]. The mechanical loss can be expressed as

$$P_{fw} = k_{fw1}f_s + k_{fw2}f_s^2 \quad (13)$$

where k_{fw1}, k_{fw2} are motor loss coefficients and f_s is the corresponding frequency in the stator winding.

Table II: IPMSM parameters

A. FEA Model of IPMSM

The finite element method is a better solution for the electromagnetic circuit design of PMSM [18], [19]. It consists of a computer model of a material that is thrilled and evaluated for specific results. It involves apportioning a set geometry into a mesh of trivial elements, solving for concrete variables at the nodes of these elements, and then incorporating the outcomes for the entire region. Therefore, the accuracy of the entire results depends on the shape, size, and distribution of the elements.

In this study, a three-phase IPMSM was designed with a power of 60 kW for use in an electric vehicle. As used recently by most electric vehicles, a three-phase hairpin winding for 48 slots and 8 poles was considered with different conductors' layers, and Motor-CAD software was used for the design. Design parameters of the study are given in Table II. Winding configuration has the capability of good effectiveness, small cogging torque and high flux-weakening skill with short end turns and high slot fills. It equally minimizes the manufacturing cost while reducing the end-winding lengths. To attain high power density and high torque, we considered creating a good slot/pole combination as 48 slots/8 poles to optimize the torque ripple. The model's flux distribution of 2D FEA is built, and 1/8 is adopted to reduce the simulation time as shown in Fig. 7 shows a mesh of16305 nodes and 498 elements. In order to improve computational efficiency, a smaller meshing grid is assumed in the stator, rotor and PMs.

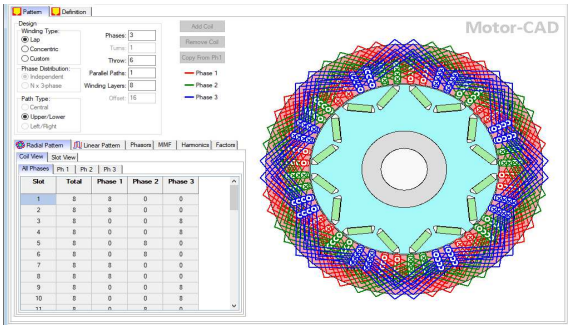

Fig. 6: Radial view of the Hairpin winding with Eight-layer motor

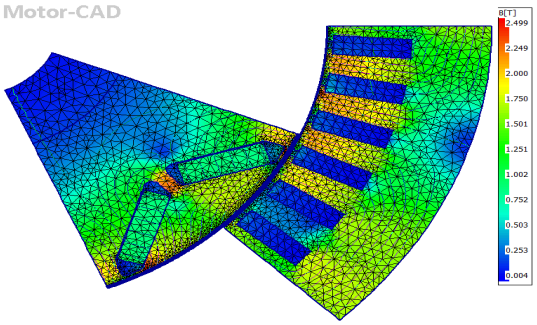

Fig. 7: The flux distribution of FEA model of the motor

Parameter	Value	Unit	Stator			Rotor		
Rated output power	60	kW	Number of slots	48	-	Outer diameter	168.5	mm
Voltage	425	V	Outer diameter	245	mm	Inner diameter	110	mm
Frequency	300	Hz	Inner diameter	170	mm	Material	M21-35A	
Speed	4500	rpm	Length	120	mm	Magnet		
Poles (N)	8	-	Material	M210-35A	-	Material	N40UH	
			Coil pitch	5	-			

IV. Results and Discussion

A. Losses of the layers

The mechanical power losses are estimated based on equation (13) and Toyota Prius motor parameters. Therefore, Table 3 compares mechanical losses in the four different layers. As observed, 8-layer is a good candidate with less loss.

Table III: Comparative analysis of mechanical loss (watt) in the layers (L) when varied in frequency at different speeds

Speed (rpm)	Frequency (Hz)	2-L (W)	4-L (W)	6-L (W)	8-L (W)
500	50	25	23	21	20
1000	60	38	35	33	32
1500	100	66	64	62	60
2000	130	117	115	112	110
2500	150	139	138	137	136
3000	200	165	164	161	160
3500	230	207	206	205	204
4000	260	248	246	245	244
4500	300	305	304	301	300
5000	330	328	326	325.6	325
5500	360	409	407	405.7	405
6000	400	479	477	476	475

B. Analysis based on 8- Layer

As observed in Fig.7, a maximum of 2.499T magnetic density distribution was formed in both the stator core and the rotor, and a homogenous flux density distribution was realized. The maximum torque ripple and the peak current of the eighth layer are presented in Fig.8. The winding harmonics is shown in Fig.9, where the higher-order harmonics are pretty low.

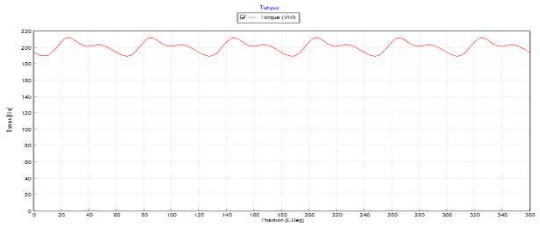

Figure 8: Maximum torque ripple

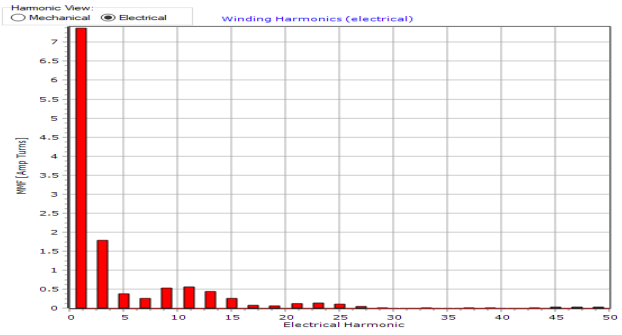

Fig. 9: Winding Harmonics order

The driving cycle is shown in Figure 10 as speed –time which is based on electric vehicle parameters in Table I. The flux weakening performance depends on the saliency ratio of the permanent magnet material. Hence, the characteristics of power verse speed and torque is shown in Fig. 11, where the maximum converter current is assumed to be 250A.

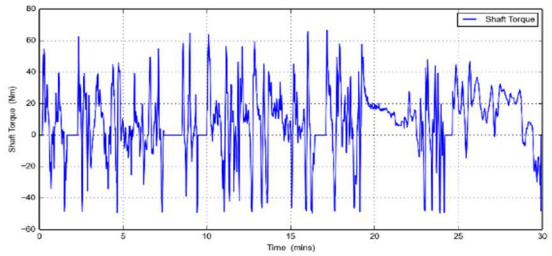

Fig. 10: Driving cycle the Electric vehicle

Figure 12 shows the efficiency map of the motor. The highest efficiency (dark red region) is 9.8E-1 and is within the speed range of 2500 rpm to 1100 rpm and a torque of 130 Nm. This is suitable for a more comprehensive operating range.

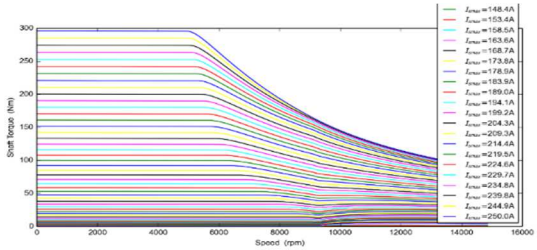

Fig. 11: Torque and power- speed characteristics

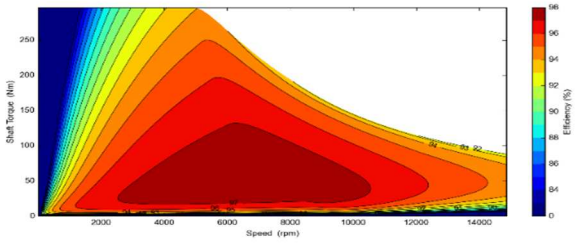

Fig. 12: Efficiency map of the motor.

V. Conclusion

The demand for high-efficiency operation of IPMSM in traction electric vehicle application is significantly on the increase. This study focuses on hairpin winding technology's contribution to improving the machine's efficiency by considering four different conduction bars in mitigating the AC winding losses. In addition, the vehicle dynamics were analysed, and the vehicle rated power of 60 kW was selected via finite element.

REFERENCES

[1] G. B. ´ Linh Dang , Nicolas Bernard, Nicolas Bracikowski, “Design Optimization with Flux Weakening of High-Speed PMSM for Electrical Vehicle Considering the Driving Cycle,” *IEEE Trans. Ind. Electron.*, vol. 64, no. 12, pp. 9834–9842, 2017.

[2] Omokhafe J. Tola, E. A. Umoh, and E. A. Yahaya, “Pulse Width Modulation Analysis of Five-Level Inverter- Fed Permanent Magnet Synchronous Motors for Electric Vehicle Applications,” *Int. J. Robot. Control Syst.*, vol. 1, no. 4, pp. 477–487, 2021, doi: 10.31763/ijrcs.v1i4.483.

[3] IEA, “Global EV Outlook 2018. Towards cross-model electrification”. In: Electric Vehicles Initiative (2018),” 2018. doi: EIA-0383(2016).

[4] A. Arzillo; S. Nuzzo; P. Braglia; G. Franceschini; D. Barater; D. Gerada; C. Gerada, “An Analytical Approach for the Design of Innovative Hairpin Winding Layouts,” in *2020 International Conference on Electrical Machines (ICEM)*, pp. 1534–1539. doi: 10.1109/ICEM49940.2020.9270927.

[5] Stefano Nuzzo; Davide Barater; Chris Gerada; Pier Vai, “Hairpin Windings: An Opportunity for Next-Generation E-Motors in Transportation,” *IEEE Ind. Electron. Mag.*, pp. 2–10, 2021, doi: 10.1109/MIE.2021.3106571.

[6] Mohammad Soltani; Stefano Nuzzo; Davide Barater; Giovanni Franceschini, “Considerations on the Preliminary Sizing of Electrical Machines with Hairpin Windings,” in *2021 IEEE Workshop on Electrical Machines Design, Control and Diagnosis (WEMDCD)*, pp. 46–51. doi: 10.1109/WEMDCD51469.2021.9425645.

[7] Phil H. Mellor; Rafal Wrobel; Neville McNeill, “Investigation of Proximity Losses in a High Speed Brushless Permanent Magnet Motor,” in *Conference Record of the 2006 IEEE Industry Applications Conference Forty-First IAS Annual Meeting*, pp. 1514–1518. doi: 10.1109/IAS.2006.256730.

[8] Faizul Momen; Khwaja Rahman; Yochan Son, “Electrical Propulsion System Design of Chevrolet Bolt Battery Electric Vehicle,” *IEEE Trans. Ind. Appl.*, vol. 55, no. 1, pp. 376–384, 2019, doi: 10.1109/TIA.2018.2868280.

[9] J. M. Terras; D. M. Sousa; A. Roque; A. Neves, “Simulation of a commercial electric vehicle: Dynamic aspects and performance,” 2011.

[10] Ahmad Ghaderi; Javad Soltani; Mohammad Ebrahimi; Amir Ali Forough Nassiraei, “Modification of electric drive vehicles performances using a direct torque control with over-modulation ability,” 2015. doi: 10.1109/IECON.2015.7392538.

[11] T. A. T. Mohd, M. K. Hassan, I. Aris, A. C. Soh, B. S. K. K. Ibrahim, and M. K. Hat, “SIMULATION BASED STUDY OF ELECTRIC VEHICLE PARAMETERS,” *ARPN J. Eng. Appl. Sci.*, vol. 10, no. 19, pp. 8541–8546, 2015.

[12] Jingnuo Yu; Jian Wang; Guihang Liang; Dong Li, “Pure electric vehicle driving system parameter matching in motor higher efficiency interval,” 2012. doi: 10.1109/ICSAI.2012.6223068.

[13] N. and R. S. Danardono Agus Sumarsono, Ghany Heryana, Mohammad Adhitya, “Performance Analysis of a Main Drive Motor—Initial Study of an EV Modeling Software Design,” *World Electr. Veh. J.*, vol. 12, no. 246, 2021, doi: 10.3390/wevj12040246.

[14] Dooyoung Yang, Hyungsoo Mok, J. Lee, and S. Han, “Adaptive Torque Estimation for an IPMSM with Cross-Coupling and Parameter Variations,” *Energies*, vol. 10, no. 167, 2017, doi: 10.3390/en10020167.

[15] E. A. Umoh and O. J. Tola, “Electronic circuit realization and adaptive control of a chaotic permanent magnet synchronous motor,” in *2nd International Engineering Conference (IEC 2017)*, 2017, pp. 395–404.

[16] O. Tola and E. A. Umoh, “Modeling and analysis of a permanent magnet synchronous generator dedicated to wind energy conversion,” in *2nd International Engineering Conference (IEC 2017)*, 2017, pp. 216–225.

[17] S. Li, S. Member, D. Han, S. Member, B. Sarlioglu, and S. Member, “Modeling of Interior Permanent Magnet Machine Considering Saturation , Cross Coupling , Spatial Harmonics , and Temperature Effects,” vol. 3, no. 3, pp. 682–693, 2017.

[18] M.N.O. Sadiku, “A simple introduction to finite element analysis of electromagnetic problems,” *IEEE Trans. Educ.*, vol. 32, no. 2, pp. 85–93, 1989, doi: 10.1109/13.28037.

[19] Jacek F. GierasRong-Jie WangMaarten J. Kamper, *Axial Flux Permanent Magnet Brushless Machines’*. AA Dordrecht, The Netherlands: Kluwers Academic, 2008.